Patterns of Alluviation in Mixed Bedrock-Alluvial Channels: 2. Controls on the Formation of Alluvial Patches

Jongseok Cho[1] and Peter A. Nelson[1]

[1]Department of Civil and Environmental Engineering, Colorado State University, Fort Collins, Colorado, USA.

Corresponding author: Peter Nelson (peter.nelson@colostate.edu)

Key Points:

- Numerical simulations are conducted in mixed bedrock-alluvial channels to analyze controls on alluvial patterns.
- Distinct alluviation patterns are observed depending on the channel slopes and initial alluviation conditions.
- The interactions between flow, bed topography, and roughness control the mechanisms of bed evolution.

Abstract

Understanding the development and spatial distribution of alluvial patches in mixed bedrock-alluvial rivers is necessary to predict the mechanisms of the interactions between sediment transport, alluvial cover, and bedrock erosion. This study aims to analyze patterns of bedrock alluviation using a 2D morphodynamic model, and to use the model results to better understand the mechanisms responsible for alluvial patterns observed experimentally. A series of simulations are conducted to explore how alluvial patterns in mixed bedrock-alluvial channels form and evolve for different channel slopes and antecedent sediment layer thicknesses. In initially bare bedrock low-slope channels, the model predicts a linear relationship between sediment cover and sediment supply because areas of subcritical flow enable sediment deposition, while in steep-slope channels the flow remains fully supercritical and the model predicts so-called runaway alluviation. For channels initially covered with sediment, the model predicts a slope-dependent sediment supply threshold above which a linear relationship between bedrock exposure and sediment supply develops, and below which the bedrock becomes fully exposed. For a given sediment supply, the fraction of bedrock exposure and average alluvial thickness converge toward the equilibrium value regardless of the initial cover thickness so long as it exceeds a minimum threshold. Steep channels are able to maintain a continuous strip of sediment under sub-capacity sediment supply conditions by achieving a balance between increased form drag as bedforms develop and reduced surface roughness as the portion of alluvial cover decreases. In lower-slope channels, alluvial patches are distributed sporadically in regions of the subcritical flow.

Plain Language Summary

Bedrock rivers may have patches of alluvial sediment that covers some or all of the underlying bedrock. The amount of this sediment cover can change dynamically over time depending on the flow, upstream sediment supply, channel morphology, and antecedent sediment conditions. Here, we use a numerical model to simulate flow and sediment transport so that we may better understand what controls sediment cover in mixed bedrock-alluvial rivers. We use the model to simulate channels of varying slopes, sediment supplies, and initial sediment cover, and we analyze the model's output to gain insight on how alluvial patches form and what controls their extent and dynamics. Our numerical model results produce phenomena that have been observed in physical experiments, and they show that the channel slope and initial sediment thickness plays an important role in determining whether and how much sediment can be deposited. Our results also show that flow transitions provide critical locations where sediment deposits can start to form. Persistent sediment cover in bedrock channels can develop when a delicate equilibrium is reached between sediment roughness and the flow field.

1 Introduction

Bedrock channels are characterized by occasional or continuous exposures of nonalluviated bedrock, which is a consequence of these channels receiving a sediment supply that is less than their transport capacity. A wide variety of models for drainage network evolution distinguish between bedrock and alluvial reaches (Howard, 1980; Howard et al., 1994; Howard & Kerby, 1983; Montgomery et al., 1996) by using channel slope and discharge to express channel transport capacity. Field investigations (Lamb et al., 2008; Massong & Montgomery, 2000; Montgomery et al., 1996; Montgomery & Buffington, 1997) demonstrate that bedrock channels occur at slopes greater than a critical value ($S > S_c$), and alluvial channels form at a slope less than the critical value ($S \leq S_c$).

The spatial distribution of alluvial cover in mixed bedrock-alluvial channels has importance for determining rates and patterns of bedrock erosion, hydrodynamics, and aquatic habitat. Mechanistic models of bedrock erosion incorporate the erosional mechanism of saltating bedload particles impacting and eroding bedrock (e.g., Demeter et al., 2005; Hartshorn et al., 2002; Sklar & Dietrich, 1998, 2001, 2004; Zhang et al., 2015), implicitly introducing dependence on sediment supply and bedrock exposure into the calculation of erosion rates. Competition between the tools and cover effects controls the spatial distribution of the bedrock channel erosion, resulting in lateral and vertical channel erosion and meandering (Finnegan et al., 2007; Lamb et al., 2015; Turowski et al., 2007; Turowski, Hovius, Meng-Long, et al., 2008; Turowski, Hovius, Wilson, et al., 2008). The cover effect is typically demonstrated by linear or exponential relations of fractional bedrock exposure as a function of sediment supply to transport capacity ratio (Sklar & Dietrich, 1998, 2004; Turowski et al., 2007). Additionally, sediment supply and alluvial cover impact the maintenance and distribution of aquatic habitat and attached micro-organisms (Buffington et al., 2004; Detert & Parker, 2010; Huston & Fox, 2015, 2016; Kuhnle et al., 2013; Lisle & Hilton, 1992; Lisle & Lewis, 1992; Madej, 2001).

Alluvial patterns in bedrock channels are controlled by spatial and temporal variations in sediment flux, transport capacity, and bed topography. These channels can exhibit alluvial patterns ranging from continuous and concentrated longitudinal strips of sediment to spatially discontinuous patches of sediment. Experiments in mixed bedrock-alluvial channels have observed spatially concentrated sediment cover and storage in low parts of the underlying bedrock topography (Finnegan et al., 2007; Johnson & Whipple, 2007), indicating that topographic roughness induces changes in local flow properties and threshold of sediment motion. Inoue et al. (2014) observed inconsistent development of alluvial cover in the inner

channel through their field experiments. Hodge and Hoey's (2016a, 2016b) experiments show that velocity is an important control on sediment deposition, as they did not observe sediment cover at low areas of the bed where the flow velocity remained high. The results from several experimental studies (Chatanantavet & Parker, 2008; Johnson & Whipple, 2010; Sklar & Dietrich, 2004; Turowski et al., 2007) suggest a few major factors control grain entrainment and bedrock exposure, such as sediment supply rate, channel slope, material size, and bed roughness.

A set of flume experiments (Chatanantavet & Parker, 2008) using different channel bed slopes has shown that for lower slopes ($S < 0.0115$) bedrock exposure decreased more or less linearly with increasing the ratio of sediment supply rate to capacity transport rate. However, for sufficiently higher slopes ($S \geq 0.0115$), the bedrock remained fully exposed when the ratio of sediment supply to transport capacity is less than a critical value, while a linear relationship between the degree of bedrock exposure and sediment supply rate to transport capacity ratio prevailed when the sediment supply exceeds transport capacity. These experiments also documented a slope-dependent "runaway alluviation," where for initially bare-bedrock conditions, low-slope channels develop linearly increasing sediment cover with increasing sediment supply, while high-slope channels remain completely exposed until sediment supply exceeds the transport capacity, beyond which the channel becomes fully alluviated. Chatanantavet and Parker (2008) suggested this may be a result of slope-dependent grain interactions; later experiments by Mishra and Inoue (2020) indicated that runaway alluviation occurred when the bedrock roughness was lower than the sediment roughness, but the gradual alluvial cover could develop when the bedrock roughness was higher than that of the sediment. A full explanation of the slope-dependent behavior of sediment dynamics in mixed bedrock-alluvial channels is still needed.

106 Morphodynamic models have struggled to replicate the types of observations made in
107 mixed bedrock-alluvial experiments. Promising results have been presented by Hodge and Hoey
108 (2012), who developed a cellular automaton (CA) model where the probability of entrainment of
109 individual grains was specified for bedrock or alluvial areas. Their model found relationships
110 between bedrock exposure and the ratio of sediment supply to transport capacity (q_s/q_c) similar to
111 those observed by Chatanantavet and Parker (2008), but in contrast to the experimental
112 observations, the majority of their CA model runs predicted that the presence or absence of
113 sediment cover on the bed at the beginning of the run did not affect the steady state sediment
114 cover. Additionally, the entrainment probabilities needed to change from run to run for their
115 results to achieve the diversity of findings Chatanantavet and Parker (2008) reported. While CA
116 models like this provide interesting insight on the potential importance of grain dynamics for
117 alluvial patterns in bedrock-alluvial channels, the absence of a flow model makes connecting
118 probabilities of sediment entrainment and deposition to physical mechanisms of sediment
119 transport and alluviation challenging.

120 Because of the complexity inherent in the roughness relationship incorporated to the flow
121 resistance and sediment transport, evaluating the relative influence of different roughness
122 mechanisms for channel evolution is currently a challenging problem. The patterns of sediment
123 cover over the bedrock bed affect the spatial distribution of local roughness, flow rate, and
124 sediment transport. Here we use a new morphodynamic model to reproduce many of the
125 phenomena that have been observed in mixed bedrock-alluvial channels, and we use the model
126 predictions to untangle the mechanisms responsible for the range of dynamic sediment behavior
127 in these environments. In particular, we use the model to investigate the following questions: 1)
128 what explains the apparent slope dependence for runaway alluviation? 2) How can mixed

bedrock-alluvial channels maintain alluvial cover when the sediment supply is less than the transport capacity? 3) How do initial conditions of sediment cover affect the temporal development of alluvial cover, and the overall relationship between bedrock exposure and sediment supply? Our results reveal the important interactions between dynamic channel roughness, flow patterns, sediment transport rates, bedform development, and alluvial cover.

2 Methods

2.1 Morphodynamic model

We have developed a two-dimensional numerical morphodynamic model for mixed bedrock-alluvial channels. The model is fully described in Cho and Nelson (submitted), and we summarize the key aspects of the model here. The model consists of three major components: (1) the 2D shallow water equations (SWE) in the depth-averaged form are applied to solve the hydrodynamical component, (2) a sediment transport model calculates bedload transport rates associated with the hydrodynamic variables and topographic variation, and (3) the modified Exner equation, which computes changes in alluvial concentration or thickness due to sediment transport divergence. The novel aspects of this model, compared to previous models applied to mixed bedrock-alluvial morphodynamics, are 1) the Exner equation of sediment continuity accounts for the volume of bedload in transport and the fraction of bed covered in sediment, 2) a composite alluvial and bedrock roughness is used in the flow calculation, 3) the friction for sediment transport is modified to account for the effects of bedforms, and 4) the numerical scheme is robust and capable of handling Froude transitions and capturing shocks. We summarize the key components of the model below.

A key assumption in most numerical models combining water flow, sediment transport, and morphological evolution is that the response time of bed evolution is relatively long compared to the timescales of relevance to the flow of water (McLean et al., 1994; Nelson et al., 2003; Tubino et al., 1999). This allows a decoupling between the water flow computation and the sediment equation by assuming a quasi-steady approximation of morphodynamic process that the bed level does not change rapidly during an infinitesimal time interval while the flow field adapts instantaneously. Thus, the decoupled model practically solves for the flow field and topographic evolution using an iterative procedure.

Mixed bedrock-alluvial channels exhibit complex roughness feedbacks due to differential roughness of alluvium and bedrock surfaces, the development of bedforms and associated form drag, as well as bed shear stress taken up by sediment transport itself. To account for this, our model uses a composite roughness partitioned into surface roughness of alluvial and bedrock bed, sediment transport roughness, and form drag. The ripple factor is applied to the shear stress to remove the form drag of the bedforms assuming the remaining part is responsible for sediment transport.

Water depth and flux are calculated using the Harten-Lax-van Leer-Contract (HLLC) scheme with the weighted average flux (WAF) method (Toro, 1992a, 1992b) and an explicit application of the central difference of the viscous and friction terms at each computational cell center in a 2D domain. Because of the local and global change in flow resistance associated with different substrate roughness between the bedrock and bed material and bedform evolution, a treatment of transcritical flow is necessary. The flow resistance consists of skin friction, form drag, and bedload transport roughness. A linear fractional cover model representing the relation between the alluvial bed and bare bedrock bed, the volume of local bed material per volume of a

monolayer of sediment grains, is used to calculate local skin friction. The form drag effect is determined using the local bed slope and topographic variation averaged over the area of interest. Additionally, the bedload layer thickness is added to the total roughness where the sediment transport occurs. The explicit calculation of each of these components of roughness is critical to be able to replicate observations of persistent sediment cover in mixed bedrock-alluvial channels (Cho and Nelson, submitted).

The bed morphology is updated using the modified Exner equation for sediment continuity (Inoue et al., 2014, 2016; Luu et al., 2004). The sediment transport capacity on the alluvial bed is estimated from Wong et al. (2007). A correction of the bedload transport rate on the pure bedrock bed is necessary considering a relatively small volume of bedload transport:

$$q_b = \begin{cases} \dfrac{V_b}{V_{bc}} q_{bc} & \text{for} \quad 0 \le V_b < V_{bc} \\ q_{bc} & \text{for} \quad V_{bc} \le V_b \end{cases} \tag{1}$$

where q_b is the bedload transport rate per unit width, q_{bc} is the bedload transport capacity per unit width, V_b is the volume of sediment per unit area in the bedload layer, and V_{bc} is the saturation volume per unit area in the bedload layer. When the bed is completely bare, only the volume of sediment in the bedload layer is brought into bedload transport without resting on the bed, referred to as the throughput bedload. When the volume of the bedload layer exceeds the saturation value, sediment starts to deposit on the bed and the linear cover fraction model is utilized to determine whether the bed is in the state of partial or complete cover:

$$\eta_a = \begin{cases} \dfrac{V_{ba} - V_{bc}}{1 - \lambda} & \text{for} \quad V_{bc} \le V_{ba} \\ 0 & \text{for} \quad 0 \le V_{ba} < V_{bc} \end{cases} \tag{2}$$

where η_a is the alluvial layer thickness, V_{ba} is the total volume of sediment per unit area in alluvial bedload layers, λ is the porosity, and

$$V_b = \begin{cases} V_{bc} & \text{for} \quad V_{bc} \le V_{ba} \\ V_{ba} & \text{for} \quad 0 \le V_{ba} < V_{bc} \end{cases} \tag{3}$$

where $V_{bc} = q_{bc}/u_s$ and u_s is the saltation velocity.

The skin friction is used for the calculation of dimensionless shear stress to account for the fact that only the near-bed grain roughness is responsible for the sediment transport, using a correction referred as to the ripple factor (Ribberink, 1987; Vermeer, 1986). The dimensionless shear stress (Struiksma, 1985; Talmon et al., 1995) and critical Shields number (Calantoni, 2002; Duan & Julien, 2005; Soulsby, 1997) are corrected for spatially varying bed topography in the direction of flow.

The critical Shields parameter calculated as a function of the ratio of the bedrock hydraulic roughness to the grain size (Inoue et al., 2014; Johnson, 2014; Mishra & Inoue, 2020) is adopted instead of constant value for bedrock and alluvial surfaces. We use a modified dimensionless critical shear stress model to simulate bed evolution in different channel slopes:

$$\tau_c^* = \alpha_c \left(k_0/d \right)^{0.6} \tag{4}$$

where α_c is the correction factor for different channel slopes, k_0 is the hydraulic roughness height, and d is the grain size.

2.2 Simulation conditions

We conducted a set of numerical experiments to explore how channel slope, initial sediment cover thickness, and sediment supply impact the evolution of patterns of alluvial cover

in mixed bedrock-alluvial channels. The simulations were designed to complement the experiments of Chatanantavet and Parker (2008) and provide mechanistic insight into controls on alluvial patterns in bedrock channels. Table 1 summarizes the initial flow and sediment condition used in each experiment based on the flume experiments conducted by Chatanantavet and Parker (2008). The computational channel is straight and longer than the experimental channel to avoid possible problems regarding bedform development sensitive to boundary disturbances. All simulations impose constant water and sediment supply, uniform sediment size, and non-erodible bedrock to exclude potential disturbances to bed topography created by unsteady conditions. The computations are stopped when near equilibrium conditions of bed topography are achieved, in which the average sediment cover thickness and the fraction of bedrock cover vary around stable values.

All simulations are performed in a rectangular bedrock channel having a length of 20 m and a width of 0.9 m. Small topographic variations with a standard deviation of 2.2 mm and peak-to-peak bed elevation of 9 mm are applied to the bedrock bed. First, two sets of simulations are performed: (1) with some initial cover thickness with different channel slopes (Runs 2-A5 and 2-B5) and (2) without antecedent sediment cover (Runs 2-Ax, 2-Bx, and 2-Dx) to explore the effect of channel slopes. Second, a set of Run 2-B is conducted with the $q_s/q_c = 0.6$ and various initial sediment cover thicknesses of 1, 4, and 6 cm. Two types of uniform grains, fine 2 mm and coarse 7 mm gravels, are employed in the experiments with a mild slope channel ($S \le 0.0115$) and with a steep slope channel ($S = 0.02$), respectively.

Table 1. Summary of Flow, Sediment Transport, and Topographic Conditions[a]

	mm		%	cm	l/s	g/s	g/s		mm	cm	cm/s	
RUN	k_b	α_c	S	Z_{bi}	Q_w	Q_c	Q_s	Q_s/Q_c	d	H	U	F_e
2-A1	0.4	0.03	1.15	1.5	24	25	5	0.2	2	4.3	62	0.78
2-A2	0.4	0.03	1.15	1.5	24	25	10	0.4	2	4.3	62	0.6
2-A3	0.4	0.03	1.15	1.5	24	25	15	0.6	2	4.3	62	0.41
2-A4	0.4	0.03	1.15	1.5	24	25	20	0.8	2	4.3	62	0.27
2-A5	0.4	0.03	1.15	1.5	24	25	25	1.0	2	4.5	59	0
2-B1	4	0.05	2	2	55	110	44	0.4	7	5	122	1
2-B2	4	0.05	2	2	55	110	66	0.6	7	5.5	111	0.4
2-B3	4	0.05	2	2	55	110	88	0.8	7	5.5	111	0.25
2-B4	4	0.05	2	2	55	110	110	1.0	7	6	102	0
2-B2-a	4	0.05	2	1	55	110	66	0.6	7	5	122	1
2-B2-b	4	0.05	2	4	55	110	66	0.6	7	6	102	0.4
2-B2-c	4	0.05	2	6	55	110	66	0.6	7	6	102	0.4
2-Ax	0.4	0.03	1.15	0	24	150	150	1.0	2	2.9	92	0
2-Bx	4	0.05	2	0	55	350	350	1.0	7	5	122	0
2-Dx-a	0.2	0.08	0.3	0	55	8	2	0.25	2	7.5	81	0.7
2-Dx-b	0.2	0.08	0.3	0	55	8	4	0.5	2	7.5	81	0.6
2-Dx-c	0.2	0.08	0.3	0	55	8	6	0.75	2	7.5	81	0.52
2-Dx-d	0.2	0.08	0.3	0	55	8	8	1.0	2	7.5	81	0

[a]The run names correspond to Chatanantavet and Parker's (2008) experimental conditions. k_b denotes bedrock roughness height, α_c denotes Shields number correction coefficient, S denotes channel slope, Z_{bi} denotes initial sediment cover thickness, Q_w denotes water discharge, Q_c denotes sediment transport capacity, Q_s denotes sediment supply rate, q_s/q_c denotes the ratio of sediment supply to transport capacity, d denotes grain size, H denotes flow depth, U denotes flow velocity, and F_e denotes the fraction of bedrock exposure, respectively.

The bedrock and grain roughness heights are back-calculated from the logarithmic law depending on the channel slope and corresponding hydraulic conditions. The spatially varying friction coefficient is then calculated as a function of the flow depth and composite roughness, which depends upon the local status of fraction cover, bedform dimension, and bedload transport

rate. The critical Shields parameters for each channel slope are back-calculated by equating the sediment transport capacity from our numerical simulations and experimental runs of Chatanantavet and Parker (2008) conducted in bedrock channels, and adjustment to the correction coefficient α_c is employed.

In each simulation, the sediment supply q_s was specified as a target fraction of the transport capacity q_c. To determine q_c, we conducted simulations for each run, assuming that the initial bed is nearly flat for either with initial sediment cover (Runs 2-A and 2-B) or bare bedrock surface (Runs 2-Ax, 2-Bx, and 2-Dx) without the presence of bedforms. The bedrock transport capacity is the lowest rate of sediment input per unit width fed into the initially bare bedrock bed that results in equilibrium conditions where the bed is completely covered ($F_e = 0$). The alluvial transport capacity is the channel averaged sediment transport rate in the alluvial channel.

3 Results

3.1 Simulations with no initial alluvial cover

Runs 2-Ax, 2-Bx, and 2-Dx all commenced with a bare bedrock bed, and are used to investigate how channel slope affects sudden vs. gradual alluviation as sediment supply increases. The lowest-slope simulations ($S = 0.003$) of Run 2-Dx exhibited a gradual decrease in bedrock exposure at increasing sediment supplies. An example of bed evolution for these runs is shown in Figure 1 for Run 2-Dx-a, for which bedrock surface roughness was 0.2 mm and the ratio of sediment supply to transport capacity was $q_s/q_c = 0.25$. The time evolution of alluvial cover illustrates that the sediment grains initially deposit in the lower topography areas, and sediment patches gradually grow thicker and expand in the upstream direction.

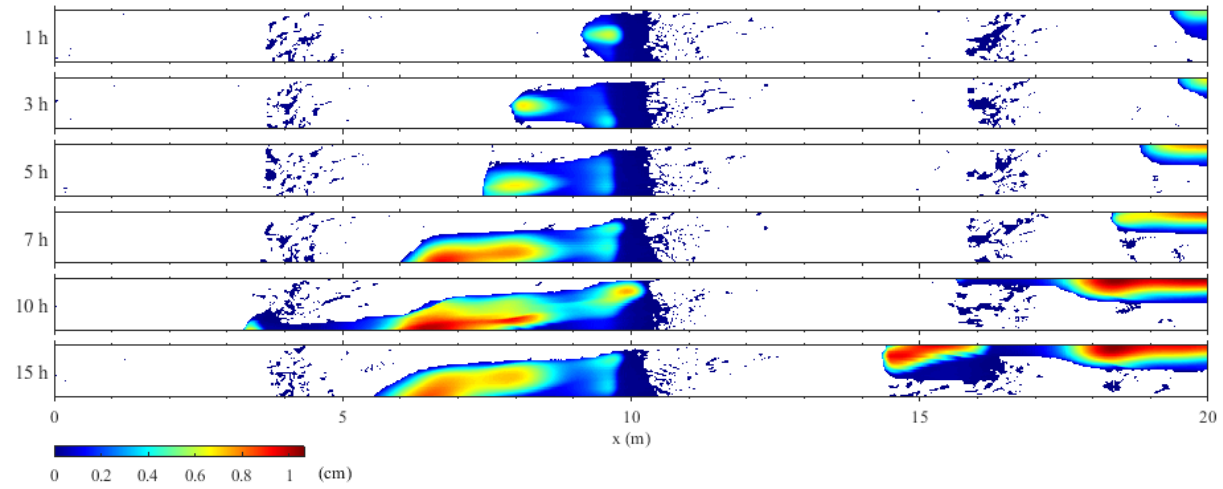

Figure 2. Simulated bed evolution of Run 2-Dx-a, which began with a bare bedrock bed and sediment supplied at q_s/q_c = 0.25. Colorbar shows the thickness of the sediment cover, and white areas correspond to the exposed bedrock surface.

Figure 2 shows the final state of alluviation for all of the low-slope 2-Dx runs. As sediment supply (i.e., q_s/q_c) increases, the alluviated patches grow in size and the overall fraction of exposed bedrock (F_e) decreases.

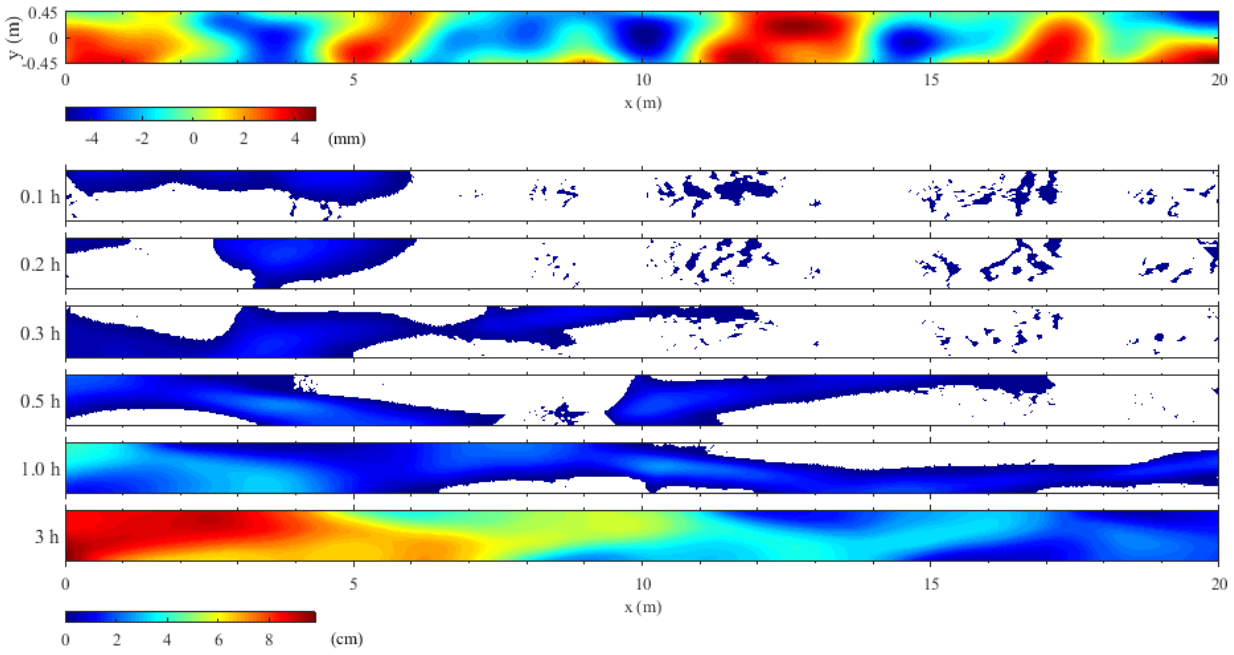

Figure 1. Plan view of bedrock topography (top). Colorbar scale indicates the detrended bed elevation. Simulated bed evolution of Run 2-Bx with q_s/q_c = 1 (bottom). Colorbar shows the thickness of the sediment cover, and white areas correspond to the exposed bedrock surface.

Figure 3 shows the time evolution of alluvial patch formation for simulation Run 2-Bx, which commenced from the bare bedrock bed in a channel with a higher slope of 0.02. For this run, bedrock roughness was 4 mm and sediment was supplied at the channel's transport capacity ($q_s/q_c = 1$). The sediment tends to deposit on the stoss side of the bedrock mounds where low flow velocity results in low Froude number, shear stress, and sediment transport capacity. The sediment forms small patches that grow in size as they move downstream. The migrating alluvial patches bypass the high bedrock areas by moving through the topographic lows. A sediment strip develops and shifts from one side of the channel to the other, and the entire channel bed is eventually covered with sediment. Complete alluviation of the bedrock bed begins from the upstream end of the channel, and alternate-bar-like patterns form as sediment moves across the channel.

Unlike the lower-slope runs of 2-Dx, simulations for 2-Ax ($S = 0.0115$) and 2-Bx ($S = 0.02$) were not able to achieve persistent alluvial cover for sediment supplies less than the transport capacity. Figure 4a demonstrates how the fraction of exposed bedrock surface varies with the sediment supply to transport capacity ratio in the initially bare bedrock channel. In steep-slope channels ($S \geq 0.0115$) without preexisting sediment, the bedrock bed remains fully

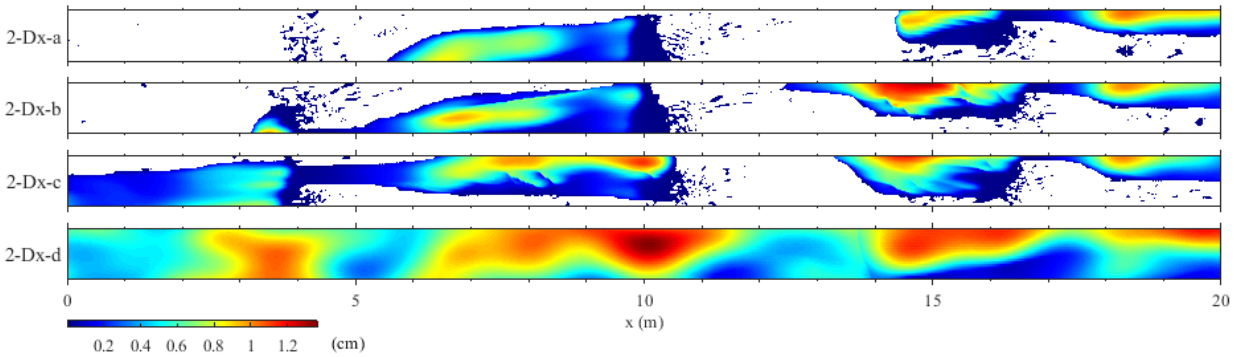

Figure 3. Plan view of Runs 2-Dx at equilibrium. The sediment is supplied at q_s/q_c = 0.25, 0.5, 0.75, and 1.0, from top to bottom. Colorbar shows the thickness of the sediment cover, and white areas correspond to the exposed bedrock surface.

277 exposed while the sediment supply rate is less than the channel sediment transport capacity.
278 When the sediment supply momentarily exceeds the threshold value, the entire bedrock bed is
279 completely covered by sediment, so-called "runaway alluviation". In contrast, in the lower slope
280 channel ($S = 0.003$, Run 2-Dx), the fractional bedrock exposure declines with increasing
281 sediment supply in a more or less linear fashion at below-capacity sediment supply. These results
282 are qualitatively and quantitatively similar to the observations of Chatanantavet and Parker
283 (2008), whose experimental results are plotted alongside ours on the same figure (Figure 4).

284 3.2 Simulations with initial alluvial cover and varying slope

285 Figure 4b compares the model-predicted and experimentally observed relationships
286 between bedrock exposure fraction and sediment supply in channels with initial sediment cover.
287 In a steeper slope channel ($S = 0.02$, Run 2-B), the bedrock is completely exposed when the
288 sediment supply to transport capacity rate is less than 0.4. However, a linear relationship
289 between the extent of sediment cover and sediment supply is exhibited when the sediment supply
290 exceeds the threshold value ($q_s / q_c > 0.6$). This threshold sediment supply rate beyond which
291 there is a linear relationship between sediment cover fraction and sediment supply ratio

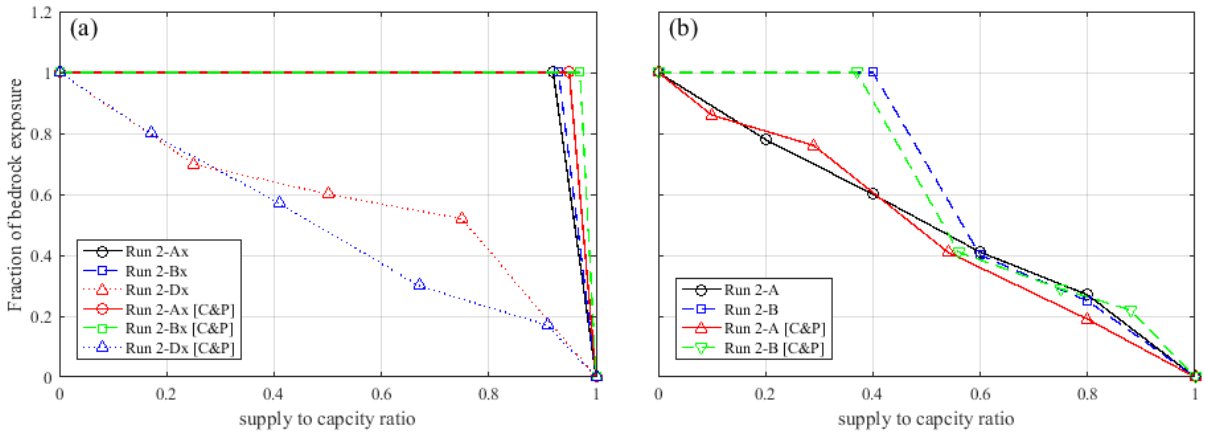

Figure 4. Results from the numerical simulations and flume experiments (Chatanantavet & Parker, 2008) of the fraction of bedrock exposure with varying sediment supply to transport capacity ratio for the simulations commenced from (a) bare bedrock channel and (b) alluvial channel.

292 decreases as the channel slope decreases (Run 2-A). In a channel slope of 0.0115, the linear
293 relationship is observed throughout the entire range of q_s/q_c that the fraction of bedrock
294 exposure increases gradually as the sediment supply to capacity ratio decreases.

295 3.3 Simulations with various initial sediment layer thickness

296 The simulations of Runs 2-B2 and 2-B2-a to 2-B2-c are conducted to explore the effect
297 of antecedent sediment layer thickness on alluvial patterns. Figure 5 shows the time evolution of
298 bedrock exposure and averaged alluvial thickness in the 2 % slope channel for both the
299 simulations and Chatanantavet and Parker (2008) experiments. The initial sediment cover
300 thickness was varied between 1 and 6 cm while the sediment flux of 66 g/s is constantly
301 supplied. In the simulation starting with 1 cm sediment cover thickness, the sediment quickly
302 erodes and washes out from the channel. The simulations with 2 cm or higher initial alluvial
303 thickness present that the fraction of bedrock exposure increases gradually and converges
304 approximately at 0.4. For those runs, the mean alluvial layer thickness over the sediment-covered
305 area evolves toward 2 cm when the initial cover thickness equals or exceeds 2 cm.

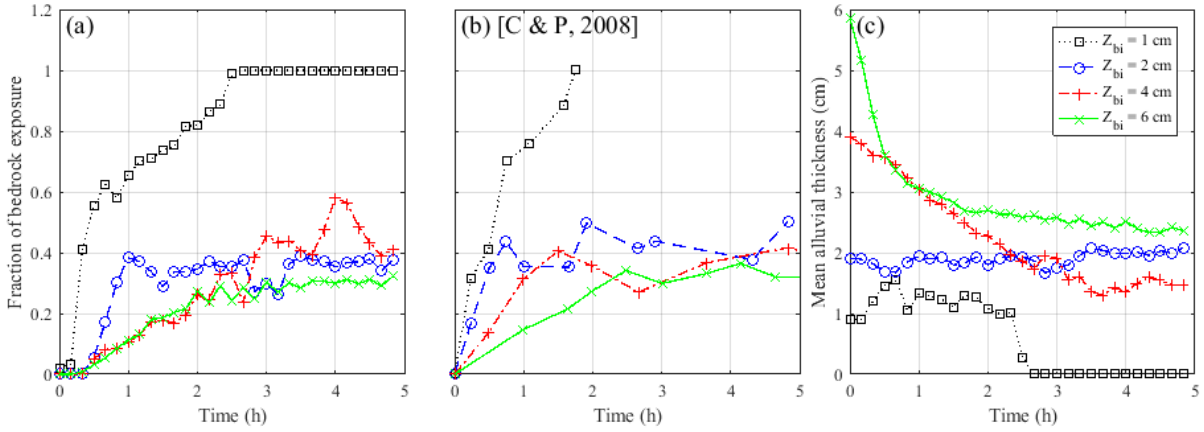

Figure 5. The time evolution of the (a) fraction of bedrock exposure from numerical simulations, (b) flume experiments (Chatanantavet & Parker, 2008), and (c) alluvial cover thickness averaged over the covered area only. The Runs of 2-B2-a, 2-B2, 2-B2-b, and 2-B2-c correspond to the initial cover thickness of 1, 2, 4, and 6 cm, respectively.

306 **4 Discussion**

307 Our results replicated several phenomena observed in the Chatanantavet & Parker (2008)
308 experiments: 1) runaway alluviation for high-slope channels with no initial sediment cover, and
309 gradual alluviation for low-slope channels with no initial sediment cover (Figure 4a), 2) a
310 threshold sediment supply for higher-slope channels with the initial cover below which sediment
311 washes out, but above which a linear relationship between sediment supply and fraction exposure
312 develops (Figure 4b), and 3) a threshold initial sediment cover thickness above which quasi-
313 steady sediment cover develops, but below which full bedrock exposure and sediment washout
314 occurs. The model's complete description of the hydrodynamic and sediment transport
315 conditions throughout the experiments help explain why these phenomena occurred.

316 4.1 Runaway alluviation vs. gradual alluviation

317 The gradual decrease in the fraction of bedrock exposed with increasing sediment supply
318 at the low-slope (2-Dx) condition, and the runaway alluviation at higher slopes where persistent
319 (total) sediment cover occurred only at sediment supply greater than the transport capacity, with
320 complete bedrock exposure at sediment supplies below that value, was observed in both our
321 numerical simulations and in the experiments of Chatanantavet and Parker (2008). Chatanantavet
322 and Parker (2008) suggested that this phenomenon may be in part due to sediment grain
323 interactions, such that at low slopes, frequent grain collisions lead to the development of alluvial
324 patches, which then increase local roughness and grow in size, whereas at higher slopes those
325 collisions may be less frequent and less likely to develop incipient patches. Hodge and Hoey's
326 (2012) cellular automata model runs with varying grain entrainment probability on bedrock and
327 alluvial surfaces suggest that the much higher grain entrainment probability on the bedrock
328 surface than the alluvial surface is a key factor of runaway alluviation.

Our model treats sediment transport as a continuum and is therefore not able to model grain interactions directly, but it still exhibited the same sort of slope-dependent relationship between gradual vs. runaway alluviation. Our model results suggest this is a result of the development of transcritical flows over bare low-slope beds, but not in higher-slope channels.

Figure 6 shows the Froude numbers calculated in the bare bedrock channel before feeding sediment at the inlet for the Runs 2-Ax, 2-Bx, and 2-Dx. The flow is supercritical in steep slope channels (2-Ax and 2-Bx), while locally subcritical flow is observed in lower slope channels (2-Dx). The flow field variables and shear stress result in a low sediment transport capacity where the flow is subcritical in the low-slope channel (Figure 7). These subcritical zones become areas of deposition, inducing a cascade of local changes in roughness, velocity, shear stress, and critical dimensionless shear stress which permit the growth of alluvial patches. However, in the steep slope channels, the large sediment transport capacity produced by high flow velocity and shear stress results in the particles passing through the channel reach without ever residing on the bed when the sediment supply is less than the transport capacity (Figure 4a).

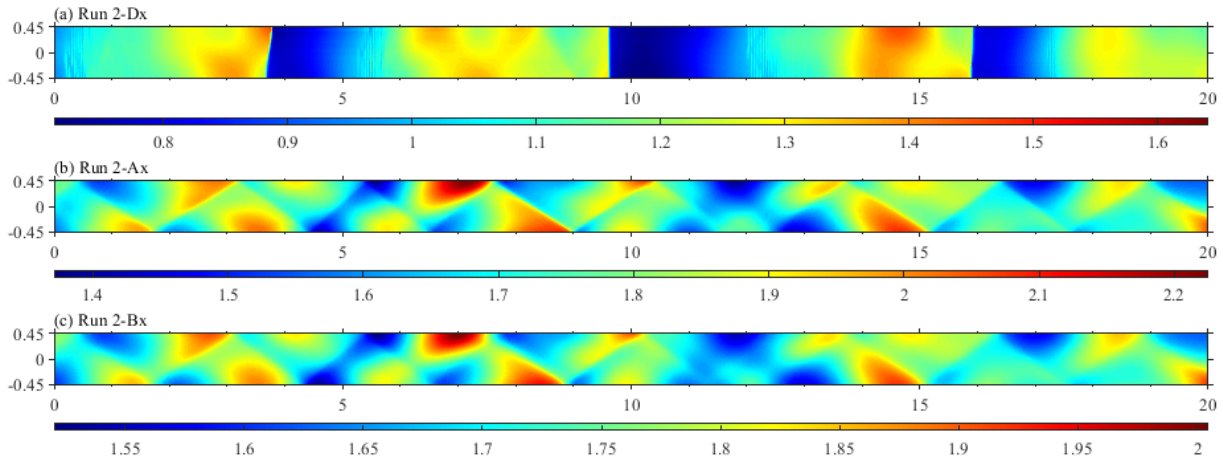

Figure 6. Initially calculated Froude number for Runs (a) 2-Dx, (b) 2-Ax, and (c) 2-Bx in bare bedrock channel. Colorbars indicate the scale of computed values, respectively.

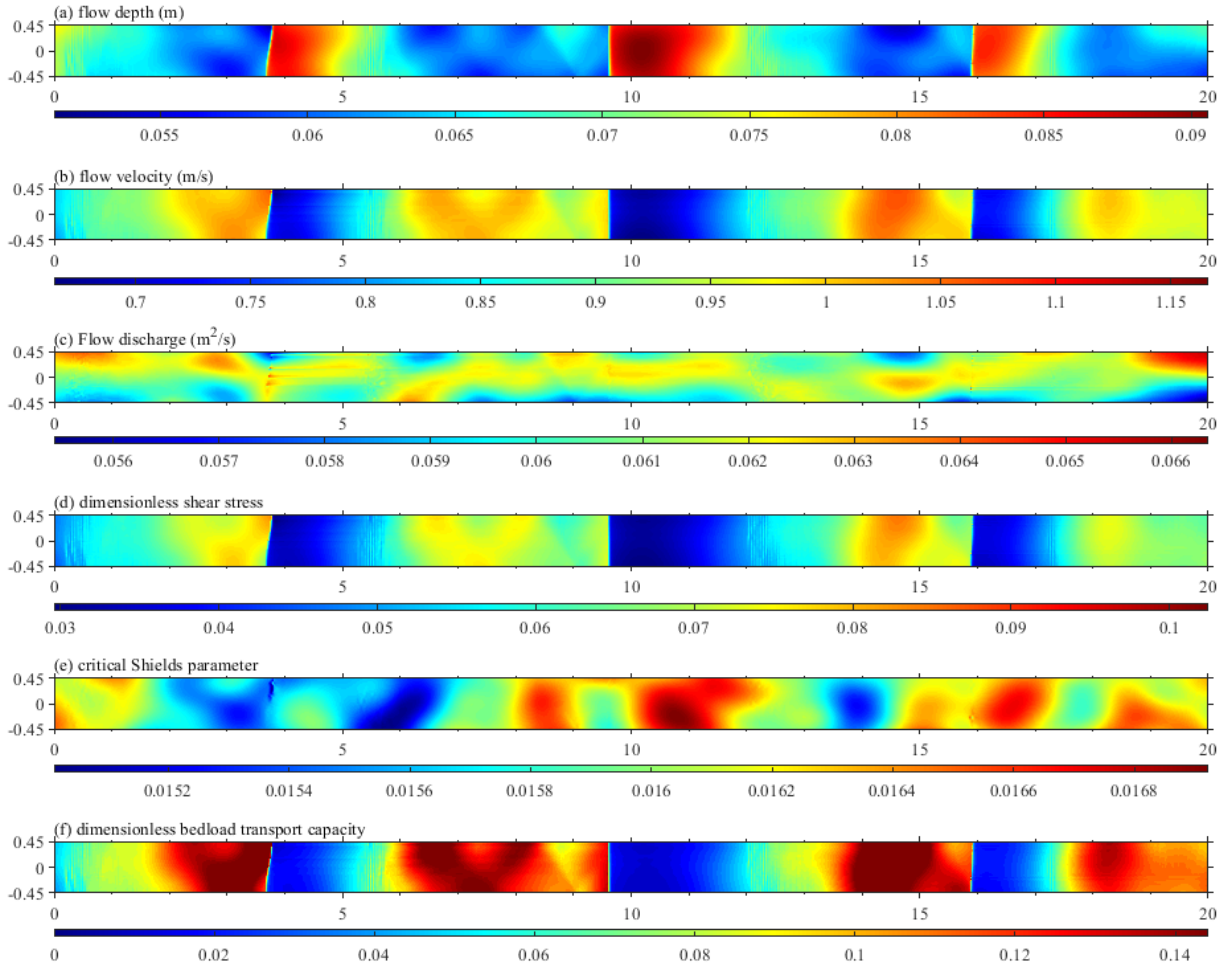

Figure 7. Initially calculated variables in bare bedrock channel for the Run 2-Dx: (a) flow depth, (b) flow velocity, (c) flow discharge, (d) dimensionless shear stress, (e) critical Shields parameter, and (f) dimensionless bedload transport capacity. Colorbars indicate the scale of computed values, respectively.

Thus, while grain interactions and roughness feedbacks may play a role in developing persistent alluvial sediment cover at below-capacity sediment supply in low-slope channels, the flow field – especially the presence of regions of transcritical flow – may be a necessary and important condition leading to this behavior.

4.2 Sediment supply threshold for persistent alluvial patches

The 2 % slope channel simulations with 2 cm initial cover thickness (Runs 2-B1, 2-B2, 2-B3, and 2-B4) show sediment washing out when the sediment supply rate is less than the

threshold capacity of about . The sediment forms alternate bars that produce additional resistance to the flow. The increased form drag roughness competes with decreased bed surface roughness due to exposed bedrock beds. The channel experiences complete bedrock exposure when the sediment supply does not meet the threshold amount to maintain the bedform. In other words, the sediment supplied to the system is redistributed to create bedforms which increase overall roughness and encourage sediment deposition and persistence of the alluvial cover; if the supply is insufficient to build the bedforms, the overall roughness decreases as bedrock becomes exposed and all of the sediment washes out (Figure 8).

Similar mechanisms explain the relationship between the initial thickness of sediment cover and the development of persistent alluvial cover as opposed to sediment washout at below-threshold initial thicknesses (Figure 5). The 1.15 % slope channel simulations with 1.5 cm initial cover thickness (Runs 2-A1 through 2-A5) show the linear relationship between the fraction cover and sediment supply to transport capacity. Transcritical flow is observed in this simulation (Figure 9). The flow is subcritical in the alluvial area and supercritical over the bedrock surface. The sediment forms a series of discrete sediment patches with a thin layer rather than a

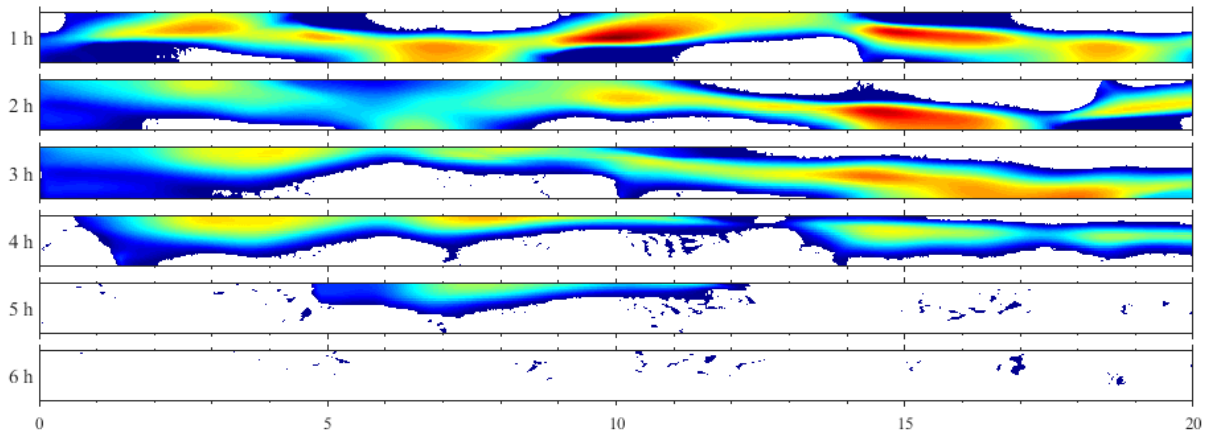

Figure 8. Simulated bed evolution of Run 2-B1 with $q_s/q_c = 0.4$. Colorbar shows the thickness of the sediment cover, and white areas correspond to the exposed bedrock surface.

365 continuous strip of sediment. The subcritical flow promotes the thin layer of alluvial patches to
366 form even in low sediment supply channels.

367 Figure 10 shows how roughness changes from the initial value of grain and sediment
368 transport roughness, form drag, and total hydraulic roughness through time. The non-bedform

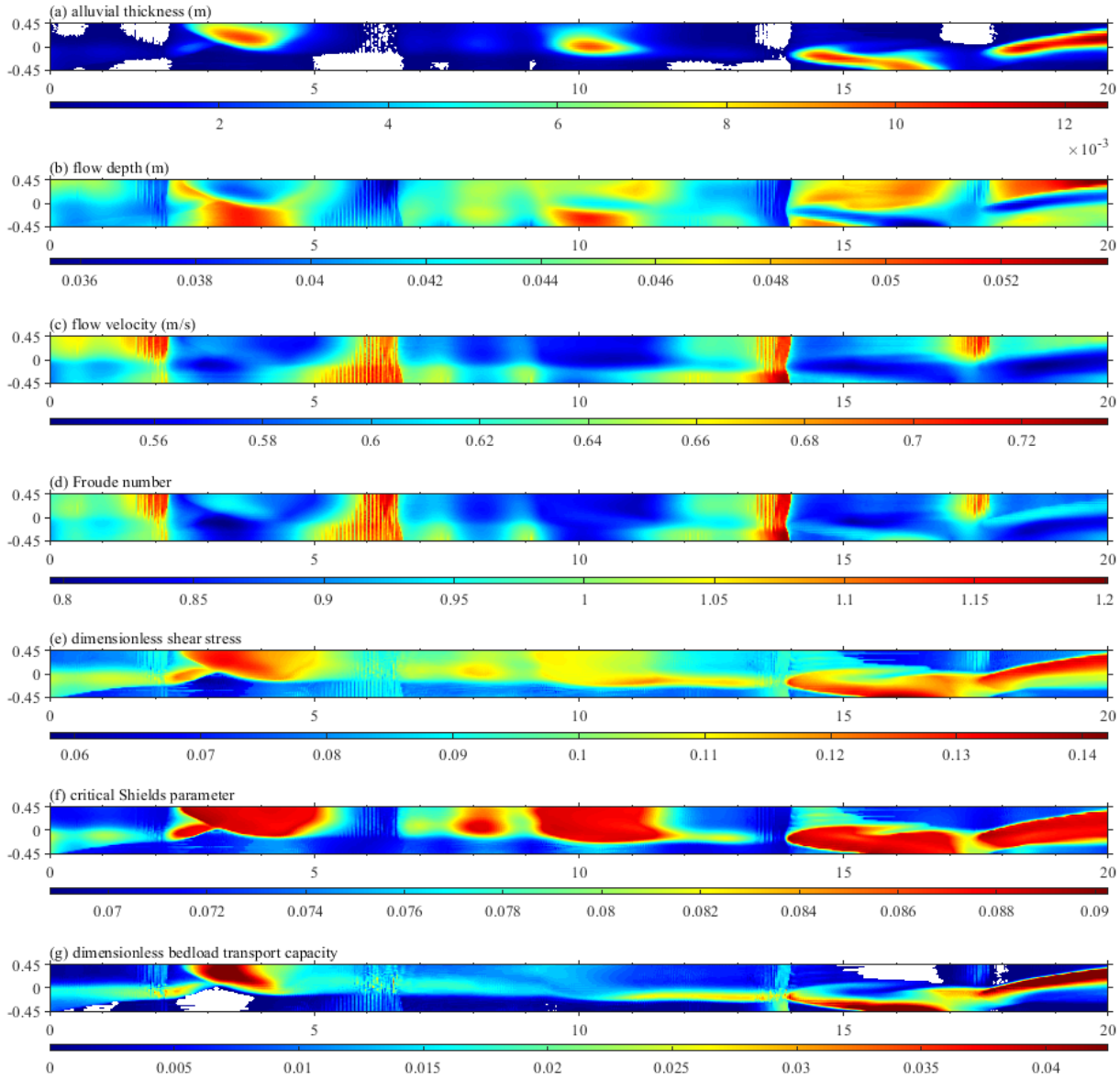

Figure 9. Simulation results commenced from alluvial channel for the Run 2-A2 at t = 5 h: (a) alluvial thickness, (b) flow depth, (c) flow velocity, (d) Froude number, (e) dimensionless shear stress, (f) critical Shields parameter, and (g) dimensionless bedload transport capacity. Colorbars indicate the scale of computed values, respectively. White areas correspond to (a) the exposed bedrock surface and (g) no bedload transport.

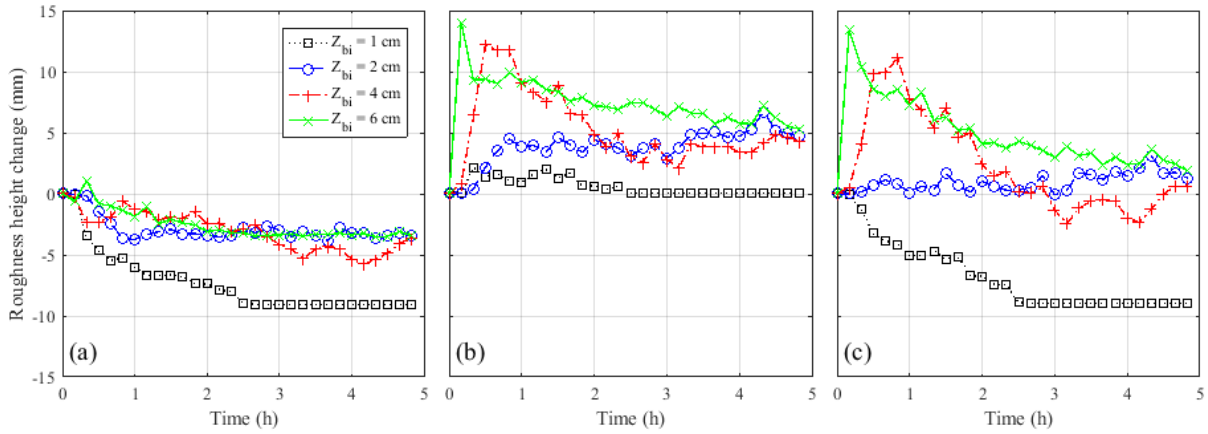

Figure 10. The time evolution of roughness difference from the initial roughness value: (a) bed surface roughness, (b) bedform roughness, and (c) total hydraulic roughness. The Runs of 2-B2-a, 2-B2, 2-B2-b, and 2-B2-c correspond to the initial cover thickness of 1, 2, 4, and 6 cm, respectively.

roughness gradually decreases as bedrock exposure increases for all Runs of 2-B2. However, the bedform roughness of Runs 2-B2, 2-B2-b, and 2-B2-c increases to 5 mm at the equilibrium state, whereas the bedform roughness of Run 2-B2-a increases at the early stage and decreases back to 0. The changes in total roughness height indicate that the channel initially requires a thicker sediment cover layer than the threshold value to develop bars and maintain alluvial strips, or sediment washing out occurs.

5 Conclusions

We used a two-dimensional morphodynamic model to conduct a series of numerical experiments in the mixed bedrock-alluvial channel. This study explores the interaction between bedrock alluviation and morphological evolution. Simulations with varying sediment supply are conducted in different slope and antecedent channel conditions. The model replicated observations from a mixed bedrock-alluvial experiment (Chatanantavet & Parker, 2008), including a) the relationship between channel slope and gradual vs. runaway alluviation, b) the slope-dependent sediment supply threshold for development of persistent alluvial cover, c) the relationship between decreasing bedrock exposure and increasing sediment supply, and d) the

development of constant alluvial cover thickness regardless of initial sediment thickness, provided the initial thickness exceeds a minimum value necessary to maintain bedform dimensions.

The model results provide physical insight on the mechanisms responsible for these phenomena. Transcritical flow plays an important role in initiating sediment deposition over initially bare bedrock, and the development of transcritical zones in low-slope simulations but not high-slope simulations may explain the apparent slope dependence of runaway alluviation. Persistent sediment cover in high-slope channels is possible when rough alluvial surfaces balance the extent of lower-roughness bedrock surfaces, and steeper channels require higher sediment supply to exceed an apparent threshold where that balance can occur.

Open Research

The output data from numerical simulations used in this analysis can be found at https://github.com/rcemorpho/morph2d.

References

Buffington, J. M., Montgomery, D. R., & Greenberg, H. M. (2004). Basin-scale availability of salmonid spawning gravel as influenced by channel type and hydraulic roughness in mountain catchments. *Canadian Journal of Fisheries and Aquatic Sciences*, *61*(11), 2085–2096. https://doi.org/10.1139/f04-141

Calantoni, J. (2002). Discrete particle model for bedload sediment transport in the surf zone. In *ProQuest Dissertations and Theses*. https://search.proquest.com/docview/305510563?accountid=6180%0Ahttp://dw2zn6fm9z.search.serialssolution.com?ctx_ver=Z39.88-2004&ctx_enc=info:ofi/enc:UTF-

406 8&rfr_id=info:sid/ProQuest+Dissertations+%26+Theses+Global&rft_val_fmt=info:ofi/f
407 mt:kev:mtx:dissertati
408 Chatanantavet, P., & Parker, G. (2008). Experimental study of bedrock channel alluviation under
409 varied sediment supply and hydraulic conditions. *Water Resources Research*, *44*(12), 1–
410 19. https://doi.org/10.1029/2007WR006581
411 Demeter, G. I., Sklar, L. S., & Davis, J. R. (2005). The influence of variable sediment supply and
412 bed roughness on the spatial distribution of incision in a laboratory bedrock channel.
413 *2005 Fall Meeting of the AGU*, 2004.
414 Detert, M., & Parker, G. (2010). Estimation of the Washout Depth of Fine Sediments from a
415 Granular Bed. *Journal of Hydraulic Engineering*, *136*(10), 790–793.
416 https://doi.org/10.1061/(ASCE)HY.1943-7900.0000263
417 Duan, J. G., & Julien, P. Y. (2005). Numerical simulation of the inception of channel
418 meandering. *Earth Surface Processes and Landforms*, *30*(9), 1093–1110.
419 https://doi.org/10.1002/esp.1264
420 Finnegan, N. J., Sklar, L. S., & Fuller, T. K. (2007). Interplay of sediment supply, river incision,
421 and channel morphology revealed by the transient evolution of an experimental bedrock
422 channel. *Journal of Geophysical Research: Earth Surface*, *112*(3), 1–17.
423 https://doi.org/10.1029/2006JF000569
424 Hartshorn, K., Hovius, N., Dade, W. B., & Slingerland, R. L. (2002). Climate-driven bedrock
425 incision in an active mountain belt. *Science*, *297*(5589), 2036–2038.
426 https://doi.org/10.1126/science.1075078

Hodge, R. A., & Hoey, T. B. (2012). Upscaling from grain-scale processes to alluviation in bedrock channels using a cellular automaton model. *Journal of Geophysical Research: Earth Surface*, *117*(F1), n/a-n/a. https://doi.org/10.1029/2011JF002145

Hodge, R. A., & Hoey, T. B. (2016a). A Froude-scaled model of a bedrock-alluvial channel reach: 1. Hydraulics. *Journal of Geophysical Research: Earth Surface*, *121*(9), 1578–1596. https://doi.org/10.1002/2015JF003706

Hodge, R. A., & Hoey, T. B. (2016b). A Froude-scaled model of a bedrock-alluvial channel reach: 2. Sediment cover. *Journal of Geophysical Research: Earth Surface*, *121*(9), 1597–1618. https://doi.org/10.1002/2015JF003709

Howard, A. D. (1980). Thresholds in river regimes. In *Thresholds in Geomorphology* (pp. 227–258).

Howard, A. D., Dietrich, W. E., & Seidl, M. A. (1994). Modeling fluvial erosion on regional to continental scales. *Journal of Geophysical Research: Solid Earth*, *99*(B7), 13971–13986. https://doi.org/10.1029/94JB00744

Howard, A. D., & Kerby, G. (1983). Channel changes in badlands. *Geological Society of America Bulletin*, *94*(6), 739. https://doi.org/10.1130/0016-7606(1983)94<739:CCIB>2.0.CO;2

Huston, D. L., & Fox, J. F. (2015). Clogging of Fine Sediment within Gravel Substrates: Dimensional Analysis and Macroanalysis of Experiments in Hydraulic Flumes. *Journal of Hydraulic Engineering*, *141*(8), 1–14. https://doi.org/10.1061/(ASCE)HY.1943-7900.0001015

448 Huston, D. L., & Fox, J. F. (2016). Momentum-Impulse Model of Fine Sand Clogging Depth in
449 Gravel Streambeds for Turbulent Open-Channel Flow. *Journal of Hydraulic*
450 *Engineering*, *142*(2). https://doi.org/10.1061/(ASCE)HY.1943-7900.0001092
451 Inoue, T., Iwasaki, T., Parker, G., Shimizu, Y., Izumi, N., Stark, C. P., & Funaki, J. (2016).
452 Numerical Simulation of Effects of Sediment Supply on Bedrock Channel Morphology.
453 *Journal of Hydraulic Engineering*, 04016014. https://doi.org/10.1061/(ASCE)HY.1943-
454 7900.0001124
455 Inoue, T., Izumi, N., Shimizu, Y., & Parker, G. (2014). Interaction among alluvial cover, bed
456 roughness, and incision rate in purely bedrock and alluvial-bedrock channel. *Journal of*
457 *Geophysical Research: Earth Surface*, *119*(10), 2123–2146.
458 https://doi.org/10.1002/2014JF003133
459 Johnson, J. P. L. (2014). A surface roughness model for predicting alluvial cover and bed load
460 transport rate in bedrock channels. *Journal of Geophysical Research: Earth Surface*,
461 *119Johnson*(10), 2147–2173. https://doi.org/10.1002/2013JF003000
462 Johnson, J. P. L., & Whipple, K. X. (2007). Feedbacks between erosion and sediment transport
463 in experimental bedrock channels. *Earth Surface Processes and Landforms*, *32*(7), 1048–
464 1062. https://doi.org/10.1002/esp.1471
465 Johnson, J. P. L., & Whipple, K. X. (2010). Evaluating the controls of shear stress, sediment
466 supply, alluvial cover, and channel morphology on experimental bedrock incision rate. *J.*
467 *Geophys. Res.*, *115*, F02018. https://doi.org/10.1029/2009JF001335
468 Kuhnle, R. A., Wren, D. G., Langendoen, E. J., & Rigby, J. R. (2013). Sand transport over an
469 immobile gravel substrate. *Journal of Hydraulic Engineering*, *139*(2), 167–176.
470 https://doi.org/10.1061/(ASCE)HY.1943-7900.0000615

Lamb, M. P., Dietrich, W. E., & Venditti, J. G. (2008). Is the critical shields stress for incipient sediment motion dependent on channel-bed slope? *Journal of Geophysical Research: Earth Surface*, *113*(2), 1–20. https://doi.org/10.1029/2007JF000831

Lamb, M. P., Finnegan, N. J., Scheingross, J. S., & Sklar, L. S. (2015). New insights into the mechanics of fluvial bedrock erosion through flume experiments and theory. *Geomorphology*, *244*, 33–55. https://doi.org/10.1016/j.geomorph.2015.03.003

Lisle, T. E., & Hilton, S. (1992). The Volume Of Fine Sediment In Pools: An Index Of Sediment Supply In Gravel-Bed Streams. *Journal of the American Water Resources Association*, *28*(2), 371–383. https://doi.org/10.1111/j.1752-1688.1992.tb04003.x

Lisle, T. E., & Lewis, J. (1992). Effects of Sediment Transport on Survival of Salmonid Embryos in a Natural Stream: A Simulation Approach. *Canadian Journal of Fisheries and Aquatic Sciences*, *49*(11), 2337–2344. https://doi.org/10.1139/f92-257

Luu, L. X., Egashira, S., & Takebayashi, H. (2004). Investigation of Tan Chau Reach In Lower Mekong Using Field Data And Numerical Simulation. *PROCEEDINGS OF HYDRAULIC ENGINEERING*, *48*(5), 1057–1062. https://doi.org/10.2208/prohe.48.1057

Madej, M. A. (2001). Development of channel organization and roughness following sediment pulses in single-thread, gravel bed rivers. *Water Resources Research*, *37*(8), 2259–2272. https://doi.org/10.1029/2001WR000229

Massong, T. M., & Montgomery, D. R. (2000). Influence of sediment supply, lithology, and wood debris on the distribution of bedrock and alluvial channels. *Geological Society of America Bulletin*, *112*(4), 591–599. https://doi.org/10.1130/0016-7606(2000)112<591:IOSSLA>2.0.CO;2

McLean, S. R., Nelson, J. M., & Wolfe, S. R. (1994). Turbulence structure over two-dimensional bed forms: Implications for sediment transport. *Journal of Geophysical Research*, *99*(C6), 12729. https://doi.org/10.1029/94JC00571

Mishra, J., & Inoue, T. (2020). Alluvial cover on bedrock channels: applicability of existing models. *Earth Surface Dynamics*, *8*(3), 695–716. https://doi.org/10.5194/esurf-8-695-2020

Montgomery, D. R., Abbe, T. B., Buffington, J. M., Peterson, N. P., Schmidt, K. M., & Stock, J. D. (1996). Distribution of bedrock and alluvial channels in forested mountain drainage basins. In *Nature* (Vol. 381, Issue 6583, pp. 587–589). https://doi.org/10.1038/381587a0

Montgomery, D. R., & Buffington, J. M. (1997). Channel-reach morphology in mountain drainage basins. *Bulletin of the Geological Society of America*, *109*(5), 596–611. https://doi.org/10.1130/0016-7606(1997)109<0596:CRMIMD>2.3.CO

Nelson, J. M., Bennett, J. P., & Wiele, S. M. (2003). Flow and sediment-transport modeling. *Tools in Fluvial Geomorphology*. https://doi.org/10.1002/0470868333.ch18

Ribberink, J. S. (1987). Mathematical modelling of one-dimensional morphological changes in rivers with non-uniform sediment. *Communications on Hydraulic & Geotechnical Engineering - Delft University of Technology*, *87–2*.

Sklar, L., & Dietrich, W. (1998). River longitudinal profiles and bedrock incision models: Stream power and the influence of sediment supply. In K. J. Tinkler & E. E. Wohl (Eds.), *Rivers Over Rock: Fluvial Processes in Bedrock Channels* (Volume 107, pp. 237–260). https://doi.org/10.1029/GM107p0237

514 Sklar, L., & Dietrich, W. (2001). Sediment and rock strength controls on river incision into
515 bedrock. *Geology*, *29*(12), 1087. https://doi.org/10.1130/0091-
516 7613(2001)029<1087:SARSCO>2.0.CO;2
517 Sklar, L., & Dietrich, W. (2004). A mechanistic model for river incision into bedrock by
518 saltating bed load. *Water Resources Research*, *40*(6), 1–21.
519 https://doi.org/10.1029/2003WR002496
520 Soulsby, R. (1997). Dynamics of Marine Sands. In *Dynamics of Marine Sands*. Thomas Telford
521 Ltd. https://doi.org/10.1680/DOMS.25844
522 Struiksma, N. (1985). Prediction of 2-D bed topography in rivers. *Journal of Hydraulic*
523 *Engineering*, *111*(8), 1169–1182. https://doi.org/10.1061/(ASCE)0733-
524 9429(1985)111:8(1169)
525 Talmon, A. M., Struiksma, N., & Van Mierlo, M. C. L. M. (1995). Laboratory measurements of
526 the direction of sediment transport on transverse alluvial-bed slopes. *Journal of*
527 *Hydraulic Research*, *33*(4), 495–517. https://doi.org/10.1080/00221689509498657
528 Toro, E. F. (1992a). The weighted average flux method applied to the Euler equations.
529 *Philosophical Transactions of the Royal Society of London. Series A: Physical and*
530 *Engineering Sciences*, *341*(1662), 499–530. https://doi.org/10.1098/rsta.1992.0113
531 Toro, E. F. (1992b). Riemann Problems and the WAF Method for Solving the Two-Dimensional
532 Shallow Water Equations. *Philosophical Transactions of the Royal Society A:*
533 *Mathematical, Physical and Engineering Sciences*, *338*(1649), 43–68.
534 https://doi.org/10.1098/rsta.1992.0002
535 Tubino, M., Repetto, R., & Zolezzi, G. (1999). Free bars in rivers. *Journal of Hydraulic*
536 *Research*, *37*(6), 759–775. https://doi.org/10.1080/00221689909498510

Turowski, J. M., Hovius, N., Meng-Long, H., Lague, D., & Men-Chiang, C. (2008). Distribution of erosion across bedrock channels. *Earth Surface Processes and Landforms*, *33*(3), 353–363. https://doi.org/10.1002/esp.1559

Turowski, J. M., Hovius, N., Wilson, A., & Horng, M. J. (2008). Hydraulic geometry, river sediment and the definition of bedrock channels. *Geomorphology*, *99*(1–4), 26–38. https://doi.org/10.1016/j.geomorph.2007.10.001

Turowski, J. M., Lague, D., & Hovius, N. (2007). Cover effect in bedrock abrasion: A new derivation and its implications for the modeling of bedrock channel morphology. *Journal of Geophysical Research: Earth Surface*, *112*(4), 1–16. https://doi.org/10.1029/2006JF000697

Vermeer, K. (1986). The ripple factor in sediment transport equations. *Rep. R657/M1314-V*.

Wong, M., Parker, G., DeVries, P., Brown, T. M., & Burges, S. J. (2007). Experiments on dispersion of tracer stones under lower-regime plane-bed equilibrium bed load transport. *Water Resources Research*, *43*(3), n/a-n/a. https://doi.org/10.1029/2006WR005172

Zhang, L., Parker, G., Stark, C., Inoue, T., Viparelli, E., Fu, X., & Izumi, N. (2015). Macro-roughness model of bedrock-alluvial river morphodynamics. *Earth Surface Dynamics*, *3*(1), 113–138. https://doi.org/10.5194/esurf-3-113-2015